

# Fish-Wearable Data Snooping Platform for Underwater Energy Harvesting and Fish Behavior Monitoring

Xingling Wang, Yuxiang Shi, Peng Yang, Xinglin Tao, Shuyao Li, Rui Lei, Zhaoqi Liu, Zhong Lin Wang, and Xiangyu Chen\*

Conventional approaches to studying fish kinematics pose a great challenge for the real-time monitoring of fish motion kinematics. Here, a multi-functional fish-wearable data snooping platform (FDSP) for studying fish kinematics is demonstrated based on an air sac triboelectric nanogenerator (AS-TENG) with antibacterial coating. The AS-TENG not only can harvest energy from fish swimming but also serves as the self-powered sensory module to monitor the swimming behavior of the fish. The peak output power generated from each swing of the fishtail can reach 0.74 mW, while its output voltage can reflect the real-time behavior of the fishtail. The antibacterial coating on the FDSP can improve its biocompatibility and the elastic texture of the FDSP allows it to be tightly attached to fish. The wireless communication system is designed to transmit the sensory data to a cell phone, where the detailed parameters of fish motion can be obtained, including swing angle, swing frequency, and even the typical swing gestures. This FDSP has broad application prospects in underwater self-powered sensors, wearable tracking devices, and soft robots.

are visual analysis and acoustic monitoring technology.<sup>[11,12]</sup> The visual method based on motion videos and images brings little interference to fish, whereas the lighting requirement is an inevitable precondition, which means full-time monitoring of dynamic behavior in all the underwater conditions (clean or polluted) may be a problem.<sup>[13,14]</sup> It is important to note that the behavior and performance of fish swimming show certain regularity when they are exposed to polluted/dirty water. The detection technique based on sound wave signals has a long undersea detection distance. However, due to the finite information carried by acoustic waves and the time-delay characteristic, it is difficult to obtain real-time information of fish behaviors.<sup>[15]</sup> Therefore, it is still necessary to find a different monitoring strategy that can provide real-time and high-resolution detection of fish behavior in all kinds of underwater conditions.

## 1. Introduction

The study of fish kinematics involves the interdisciplinary knowledge of biology, covering neurobiology, biomechanics, ethology, and ecology.<sup>[1–3]</sup> The comprehensive understanding of fish swimming behavior not only provides important insights into kinematics and physiology,<sup>[4,5]</sup> but also benefits the study of bionic devices,<sup>[6]</sup> underwater intelligent robots,<sup>[7,8]</sup> aquaculture, and so on.<sup>[9,10]</sup> At present, the most commonly used methods to study fish behavior

On the other hand, the development of the Triboelectric Nanogenerator (TENG) has brought out various self-powered sensor and detection systems.<sup>[16–18]</sup> The high sensitivity to mechanical stimuli makes TENG suitable for recording various motion and muscle information.<sup>[19]</sup> TENG has many advantages, such as simple structure, low manufacturing cost, high energy conversion efficiency, and so on.<sup>[20]</sup> Abundant TENG-based devices,<sup>[21,22]</sup> such as electronic skin, self-powered sensors, energy harvesters, have emerged considerably.<sup>[23]</sup> Meanwhile, soft materials such as silicone, polydimethylsiloxane (PDMS), and textiles have become favored materials for the production of TENG recently,<sup>[24–27]</sup> making TENG suitable for monitoring muscle movement, respiratory rate, and pulse wave.<sup>[28–32]</sup> For some extreme cases, the sensitivity of TENG-based wearable sensors can even reach 5.16 V/0.01°.<sup>[33]</sup> Hence, a self-powered system based on the combination of TENGs and flexible waterproof materials can be used as a new approach to track fish movement patterns in a water environment. However, the wearable sensor designed for a human may not be easily adapted to the fish body, while the screen effect of the water also jeopardizes the stability. Furthermore, fish movements are more irregular and strenuous than humans and the underwater environment is full of uncertainty. Therefore, it is necessary to have a sensor with better robustness, lightweight, and flexibility to fit fish bodies.<sup>[34,35]</sup>

Here, for the first time, we applied TENG in the field of fish kinematic monitoring. A fish-wearable data snooping platform

X. Wang, Y. Shi, P. Yang, X. Tao, S. Li, R. Lei, Z. Liu, Z. L. Wang, X. Chen  
CAS Center for Excellence in Nanoscience  
Beijing Key Laboratory of Micro-nano Energy and Sensor  
Beijing Institute of Nanoenergy and Nanosystems  
Chinese Academy of Sciences  
Beijing 100083, P. R. China  
E-mail: chenxiangyu@binn.cas.cn

X. Wang, Y. Shi, P. Yang, X. Tao, S. Li, R. Lei, Z. Liu, Z. L. Wang, X. Chen  
College of Nanoscience and Technology  
University of Chinese Academy of Sciences  
Beijing 100049, P. R. China

Z. L. Wang  
School of Materials Science and Engineering  
Georgia Institute of Technology  
Atlanta, GA 30332, USA

 The ORCID identification number(s) for the author(s) of this article can be found under <https://doi.org/10.1002/sml.202107232>.

DOI: 10.1002/sml.202107232

(FDSP) has been proposed for investigating fish kinematics performance through real-time and wireless sensory techniques. The FDSP is manufactured based on the combination of an air-sac TENG (AS-TENG), the antibacterial nano-coating, and a wireless signal transceiver module, where the remote monitoring of fish motion can be achieved. The post-sputtering treatment is applied on Polytetrafluoroethylene (PTFE) film for introducing C=C bonds on the molecular chain, which allows the AS-TENG to provide a high output voltage during the swinging motion of the fishtail. Combined with the airbag structure, this AS-TENG can work as a highly sensitive motion sensor for monitoring real-time fish behavior. Moreover, the silica-functionalized quaternary ammonium compounds (Fixed-Quat) coating is deposited on the skin-integrated sleeve for eliminating bacterium and the buoyant force from the air sac can reduce the weight burden of the system, both of which improve the biocompatibility of the FDSP. Related experiments are carried out on both the fishtail model and the real fish. Benefits from its characteristics like water tightness, ideal flexibility, and output performance, the FDSP greatly expands the underwater applicability of TENGs as wearable electronics in submarine scenarios.

## 2. Results and Discussion

Extensive research has been carried out on fish kinematics during the past couple of decades.<sup>[36–38]</sup> It has been reported that over 70% of the instantaneous force in Fast-start swimming

is generated by the tail rather than the fins, while the different characteristics of fishtail oscillations can be used to identify the motion state and specific moving postures of fish,<sup>[39,40]</sup> which inspires us to colledge the information from moving fishtail to monitor fish behaviors. Accordingly, an FDSP that can be integrated onto the fishtail has been designed, which is shown in **Figure 1a**. The entire FDSP is composed of an AS-TENG as the mechanical sensory module, a wireless transceiver module, and a power management unit (see **Figure 1b**). Silicone is selected as the encapsulation material for FDSP due to its flexibility, stretchability, and malleability, which facilitates the FDSP to attach to the fishtail skin fittingly. Moreover, to maintain the biocompatibility for this FDSP, an antibacterial coating is chosen to be coated upon the surface of the silicone sheath (**Figure 1c**). Quaternary ammonium compounds (QACs) are common cationic surfactants mainly used for food and medical disinfection.<sup>[41]</sup> In this work, a Fixed-Quat active surface is adopted on the wearable FDSP to control the amount of released QACs in water,<sup>[42]</sup> to achieve the antibacterial condition in specific areas. Here, the concept of the FDSP is demonstrated in **Figure 1d**, where the mechanical energy can be captured by the AS-TENG, and the motion information can be transmitted to a mobile receiver via a wireless transceiver module, leading to the real-time sensing of fish behavior.

The AS-TENG has been designed as an airbag structure, which is illustrated in **Figure 2a**. Such hollow design not only reduces its weight and lowers the resistance to the normal movement of fish, but also maintains a stable operation of TENG regardless of the surrounding water environment. The airbag

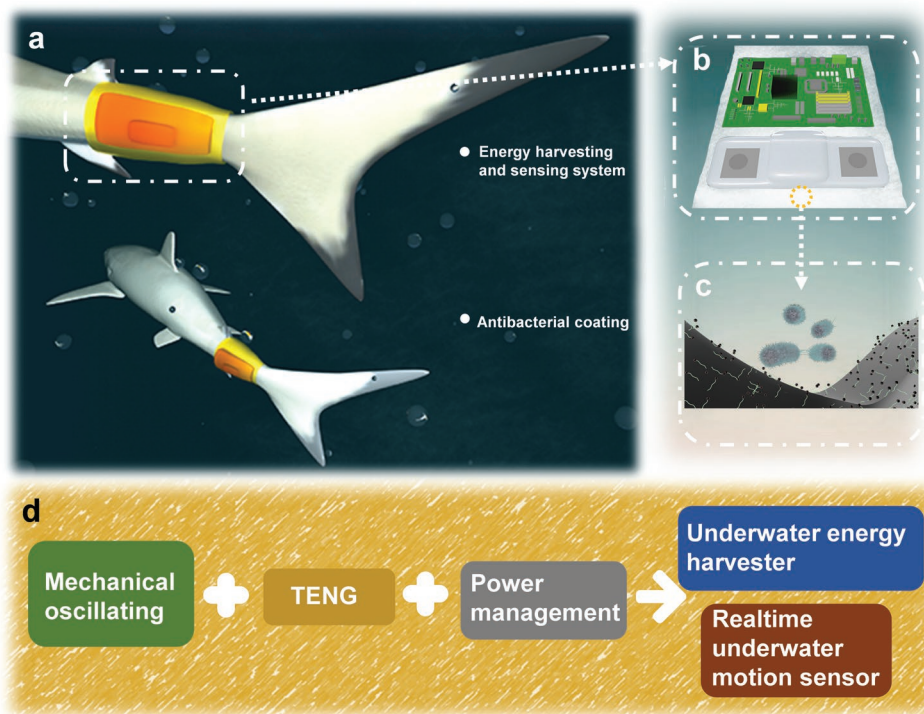


**Figure 1.** Schematic diagram of the wireless fish-wearable data snooping platform (FDSP). a) Principle, functions, and application scenarios of the FDSP. b) Schematic diagram of the structure of the FDSP. c) Schematic diagram of the structure of the antibacterial Fixed-Quat coating and the sterilization principle (contact-killing mechanism). d) The conception of the fish-wearable data snooping platform consists of three parts.

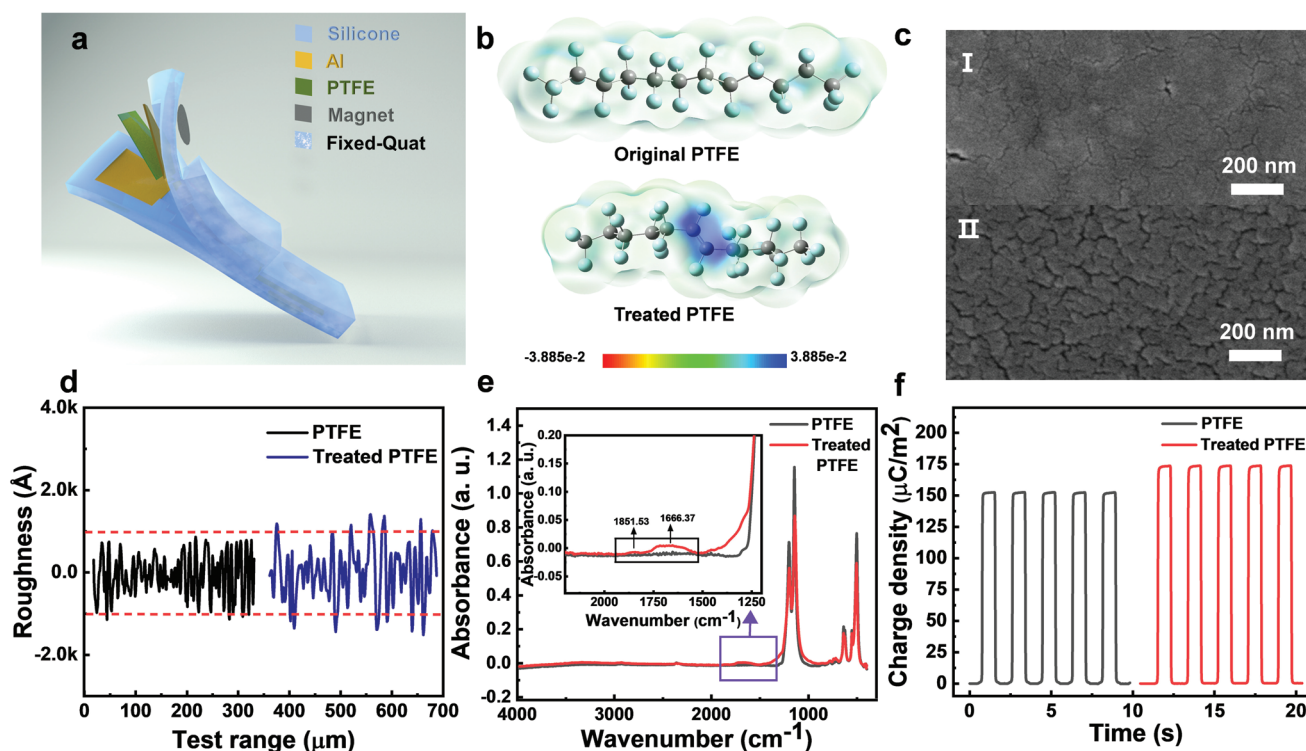


**Figure 2.** Structural design of AS-TENG and the characterization of the sputtered PTFE. a) Schematic diagram of the AS-TENG, which is mainly composed of silicone, PTFE films, aluminum foil electrodes, magnet sheets, and Fixed-Quat coating. b) 3D plots of the molecular electrostatic potential map of pristine  $C_{12}F_{26}$  (simulating PTFE) and treated PTFE. c) The scanning electron microscopy image of the pristine PTFE (I) and treated PTFE (II), the scale in the picture is 200 nm. d) Comparison image of the roughness between the pristine PTFE and treated PTFE. e) The ATR-FTIR spectra of pristine PTFE and treated PTFE film. f) Surface charge density of pristine PTFE and treated PTFE film, respectively.

contains two contact-separation mode TENGs, each of which consists of two aluminum (Al) foil electrodes ( $2\text{ cm} \times 2\text{ cm}$ ), and a PTFE film acted as a dielectric layer. It has been reported that the double bond of  $C=C$  on the molecular chain can possibly change the electrification capability of the polymer.<sup>[43,44]</sup> In order to study the influences of  $C=C$  bonds to the electrification capability of PTFE, the 3D electrostatic potential simulation is employed, as illustrated in Figure 2b. The existence of unsaturated group ( $C=C$  bonds) on the molecular chain can clearly induce a region with high electrostatic energy, indicating stronger electron-withdrawing ability. Meanwhile, for the PTFE molecule, the unsaturated groups of molecular chains contain a lot of  $C=C$  bonds. Hence, the post-sputtering method has been used to introduce unsaturated bonds ( $-CF=CF-$  or  $-CF=CF_2$ ) onto the molecular chains. A 200 nm layer of PTFE is sputtered onto the pristine PTFE film and the change in electrical properties of the treated PTFE has been tested. A comparison between the morphology of the pristine PTFE and treated PTFE is shown in Figure 2c, with surface roughness of  $\pm 100\text{ nm}$  and  $140\text{ nm}$  (Figure 2d), respectively. The ATR-FTIR spectrum result shows two new peaks in the treated PTFE at  $1550\text{--}1892\text{ cm}^{-1}$ , relating to the unsaturated groups appearing in the middle ( $1666.37\text{ cm}^{-1}$ ) and end ( $1851.53\text{ cm}^{-1}$ ) of the main chain (Figure 2e). Accordingly, as can be seen in Figure 2f, the surface charge density between Al and different PTFE layers (pristine PTFE and treated PTFE) is  $152.3\text{ }\mu\text{C m}^{-2}$  and  $173.6\text{ }\mu\text{C m}^{-2}$ , which is in good agreement

with the theoretical simulation. The flexible and stretchable silicone rubber coated with Fixed-Quat coating is used as the encapsulation material to form a hollow airbag, which has the ability to resist the interference from the underwater environment. Particularly, magnets are embedded in the middle of the silicon rubber wrapped around the electrodes, which ensures TENGs can contact well and realize effective contact electrification during underwater operation, playing an unparalleled role in enhancing the output performance. The detailed production process, size, and photograph of the AS-TENG can be found in Figure S1 (Supporting Information).

To achieve a precise perception of fish oscillations, the airbag is divided into three chambers connected by two venting channels. The structure of the chambers and channels is asymmetrical up and down, which allows TENG to have an air gap surrounding even in the tight contact condition and contribute to the smooth flow of air inside the airbag. The working principle of AS-TENG is based on the coupling effect of contact electrification and electrostatic induction.<sup>[45]</sup> The operation principle of the airbag is shown in (Figure S2a,b, Supporting Information). In the initial state, as the two electrodes of AS-TENG are in contact under the force of the magnets, the gas is gathered in the middle gas chamber. Then, the triboelectrification effect occurs at the contact interface, and charges in opposite polarities are generated at the surface of Al foil and PTFE film, respectively. When a mechanical pressing is applied on the middle gas chamber, the gas flows into the chambers

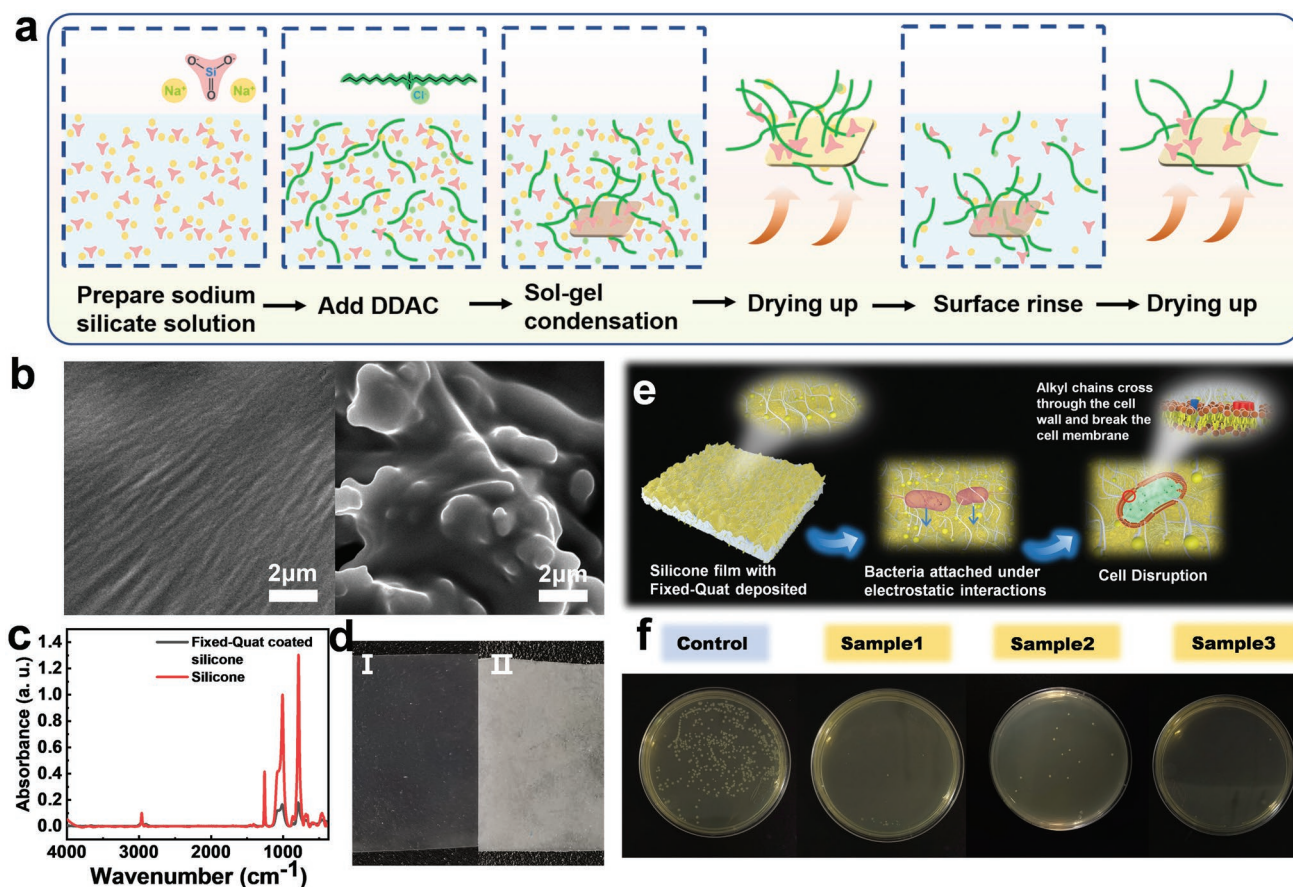


**Figure 3.** The synthesis diagram and characterization of Fixed-Quat coating. a) The synthesis and coating procedure of Fixed-Quat coating on silicone surfaces. b) The comparison of the SEM image between the pristine silicone sample (left) and Fixed-Quat coated silicone sample (right) (10 000× magnification at 10 kV). c) The infrared spectrum of uncoated silicone sample and Fixed-Quat coated silicone sample. d) Photographs of the pristine silicone sample (I) and Fixed-Quat coated silicone sample (II). e) Schematic diagram of the sterilization principle (contact killing mechanism) of the Fixed-Quat coated silicone sample for *E. Coli* disinfection. f) Optical images of the results of the bactericidal performance of Fixed-Quat coated silicone samples against *E. coli*.

on both sides, leading to the separation of electrodes of the TENG. During the separation of TENGs, the positive charges on the Al electrode are induced due to the electrostatic induction effect. The asymmetric charges between Al electrodes generate a potential difference between the two electrodes, driving electrons to transfer along the external circuit and creating a current signal. Due to the inherent properties of the dielectric layer, the accumulated tribo-charges persist for a long time. When the applied force is gradually released, the gas flows back to the middle chamber, resulting in a reversal current in the external circuit. The operation mode of the AS-TENG as well as the potential distributions in the cross-section at various working states can be studied by finite element simulations through COMSOL Multiphysics, as shown in Figure S2c (Supporting Information).

The preparation procedure of Fixed-Quat coating is shown in Figure 3a. The antibacterial active surface is fabricated through the sol-gel technique by the condensation of Fixed-Quat and silicone rubber, while the detailed processes can be seen in the experimental part. To characterize the changes in the topography and chemical composition, a scanning electron microscope with X-Ray Energy-Dispersive Spectrometer (EDS)

is primarily used to exam the surface of pristine silicone rubber and Fixed-Quat coated silicone rubber, the results are shown in Figure 3b and Figure S3 (Supporting Information). The pristine silicone presents a smooth and homogeneous surface, whereas the Fixed-Quat coating shows an amorphous and rough surface topology. The increasing composition of N, O, and Cl elements showed in the EDS analysis (Figure S3 and Table S1, Supporting Information) indicates that the coating is successfully deposited on the surface. Fourier infrared spectroscopy (FTIR) is utilized to exam the chemical attachment changes as well, which is shown in Figure 3c. The difference between the two samples can also be identified by the observation from the large scale (Figure 3d). The sterilization mechanism of the Fixed-Quat coating is illustrated in Figure 3e. The electrostatic interactions occur between the cationic groups in the QAC molecule and the negatively charged plasma membrane of the microorganism,<sup>[42]</sup> thus electrostatically anchoring the QAC molecule on the surface of the bacterial cell, followed by the penetration of the long hydrophobic alkyl chains in the QAC molecule through the cell wall and disrupt the cells. In this experiment, *E. coli* (ATCC 25 922) is used as an indicator organism for common pathogens to be assessed. Before conducting antibacterial

experiments, the Fixed-Quat coated samples are rinsed several times with DI water to remove the suspended Si-QAC from the solution and ensure that the bactericidal property is only related to the Fixed-Quat coating (Figure S4a, Supporting Information). In the antimicrobial test, pristine silicone rubber and Fixed-Quat coated samples (2 cm × 2 cm × 1 mm) are put in PBS buffer containing an initial concentration of  $10^6$  cells  $\text{ml}^{-1}$  *E. coli*, three sets of parallel experiments are set up. Subsequently, the samples are incubated on a shaker for 24 h. The cultured solutions are taken out, diluted, plated on nutrient agar plates, and incubated for 24 h at 35 °C for viable cell counting. The results are shown in Figure 3f and Figure S4b,c (Supporting Information), where the samples coated with Fixed-Quat demonstrated great sterilization of *E. coli*, with a bactericidal rate of >97%. In addition, sterilization time is taken into account, samples are removed at specific time intervals (every 8 hours) for bacterial culture and cell counting (see Figure S4d,

Supporting Information). It can be seen that there is no significant increase in bactericidal efficiency at the 16th and 24th hours, indicating that the coating can achieve a remarkable bactericidal effect against *E. coli* within 16 h. The above experimental tests are performed in a biosafety cabinet and all materials and chemicals are autoclaved (121 °C, 15 min).

The AS-TENG is found to have excellent output performance both in the air and underwater. When the airbag is subjected to mechanical force in the air, its open-circuit voltage ( $V_{oc}$ ) can be 225 V, short-circuit current ( $I_{sc}$ ) can reach 175  $\mu\text{A}$ , and the short-circuit transferred charge ( $Q_{sc}$ ) can be up to 75 nC (Figure 4a–c). Figure 4d demonstrates the output of AS-TENG with different external resistance underwater. As the load resistance increases, the output voltage increases accompanied by a decrease in current. In addition, the AS-TENG reaches its peak power at 0.74 mW under an external load of 20 M $\Omega$  in the water, while it has a peak power of 0.80 mW with an external load of

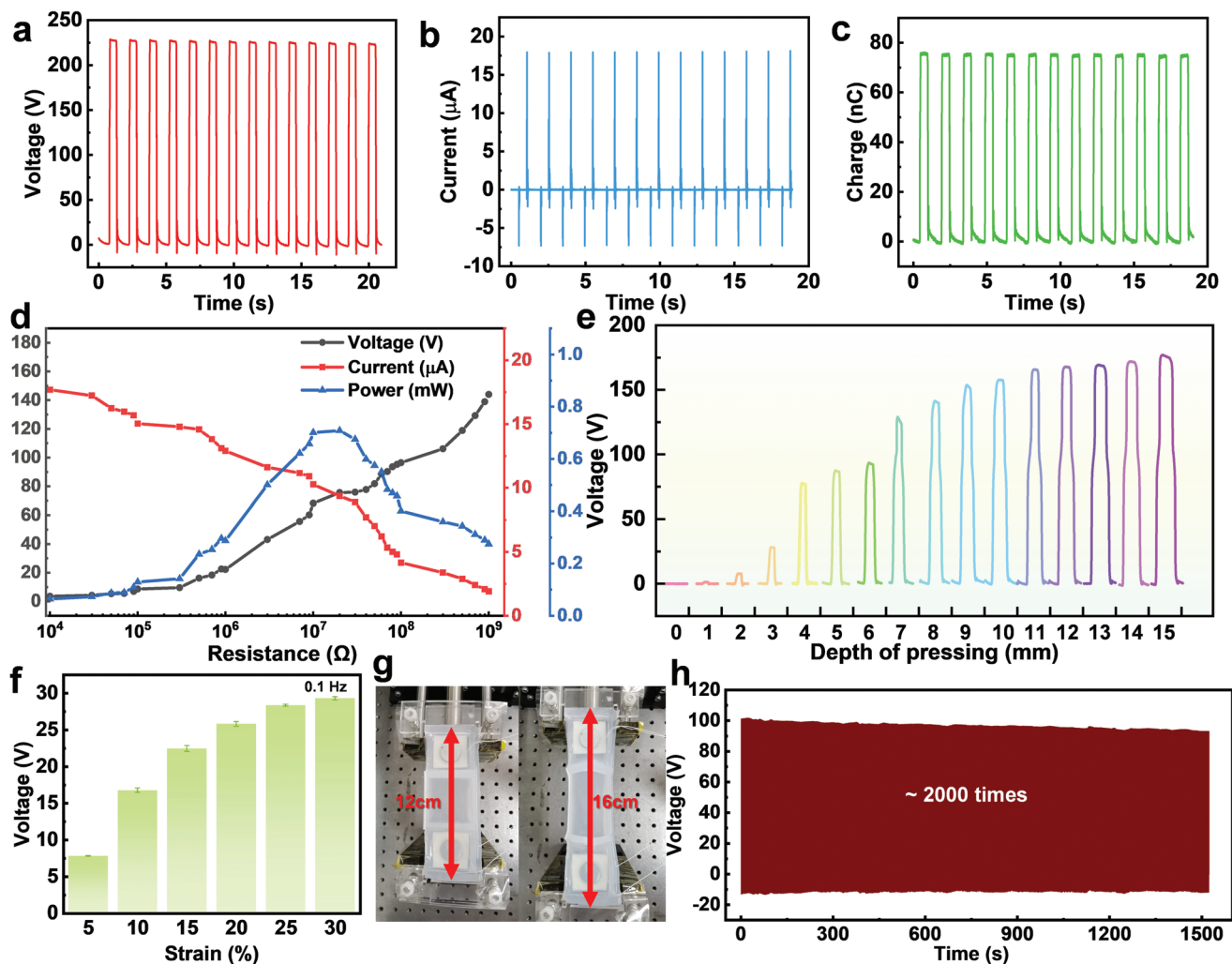


**Figure 4.** Electrical characteristics of the AS-TENG. Electrical output performance of AS-TENG when working in dry environment (controlled by a linear motor), including a) Open-circuit voltage  $V_{oc}$ , b) short-circuit current  $I_{sc}$ , and c) short-circuit charge quantity  $Q_{sc}$ . d) The variation of the output voltage, current, and output power with external load resistances in the liquid environment. e)  $V_{oc}$  of AS-TENG when working at different press depth (controlled by a linear motor). f)  $V_{oc}$  of AS-TENG when working under different strain. g) Comparison image of AS-TENG at initial state (0% strain) and stretched state (30% strain). h) Voltage of AS-TENG over  $\approx 2000$  operating cycles controlled by a linear motor.

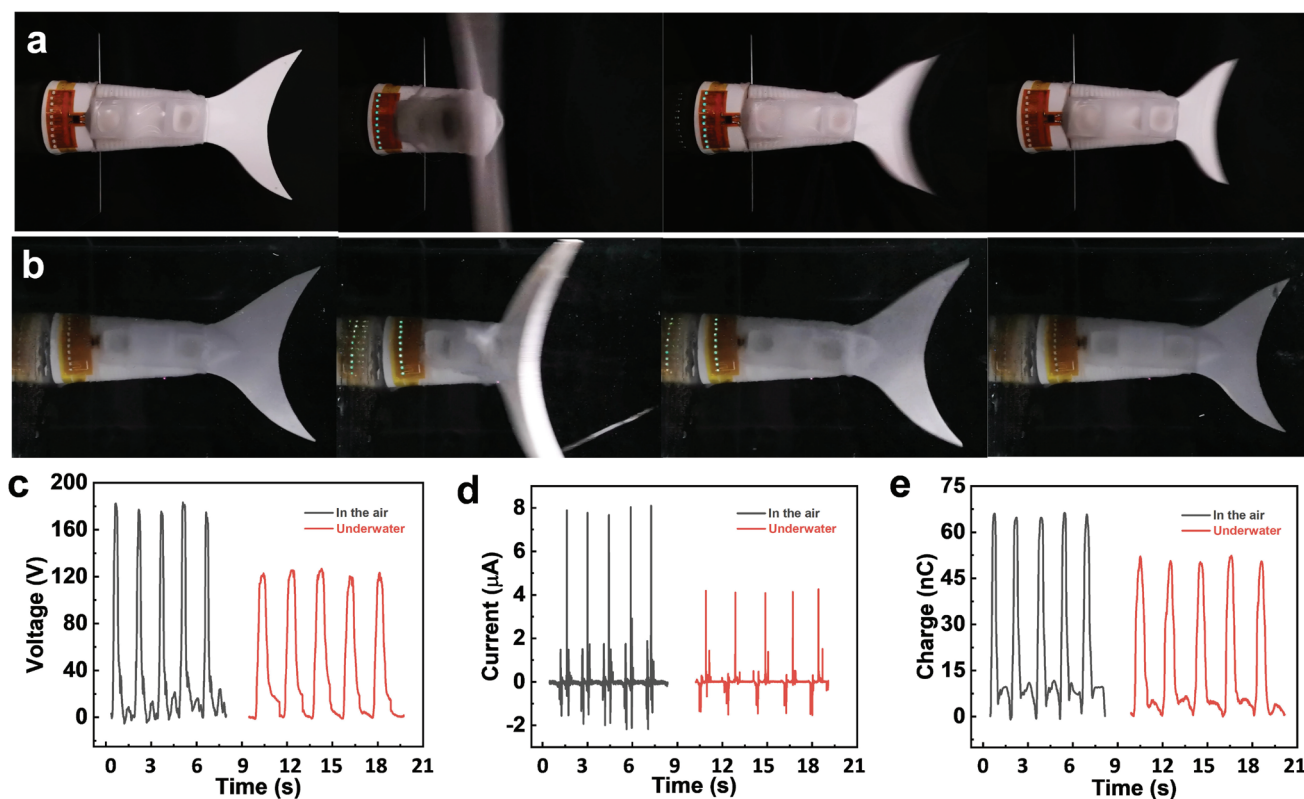


**Figure 5.** Energy harvested by the FDSP. Photographs of the LEDs-integrated FDSP worn on the fishtail model, showing that FDSP can work normally both a) in the air and b) underwater. Electrical outputs of the FDSP fixed on the fishtail model in the air and underwater, including c)  $V_{oc}$ , d)  $I_{sc}$ , and e)  $Q_{sc}$ .

20 M $\Omega$  in the air (Figure S5a, Supporting Information). Driven by a linear motor, the electric output of the AS-TENG has been characterized at different pressing depths. As illustrated in Figure 4e, the output voltage gradually rises with an increase in the depth of pressing. Owing to the stretchability of silicone rubber, the AS-TENG has good flexibility and can be stretched over 300% (Movie S1, Supporting Information). Besides, due to the asymmetry structures inside the silicone airbag, horizontal sliding friction is generated between the upper dielectric layer and the lower electrode of the AS-TENG when stretched, and its output properties are measured by uniaxial tensile experiments performed on a linear motor (Figure 4f,g; Figure S5b–e, Supporting Information). When the tensile frequency is fixed at 0.1 Hz, the  $V_{oc}$  and  $Q_{sc}$  increase as the tensile rate increases from 0% to 30% (Figure 4f; Figure S5b, Supporting Information). The change of tensile frequency is also found to have effects on the output performance of the AS-TENG, which can be seen in (Figure S5c–e, Supporting Information). In order to demonstrate the airtightness and waterproof properties, the AS-TENG together with the encapsulated light-emitting diodes (LEDs) are put into the water, where the external force applied on TENG can light up ten LEDs (Figure S6, Supporting Information). In addition, a fatigue resistance test is conducted on the AS-TENG by using a linear motor to press the AS-TENG to the half depth (7.5 mm) repeatedly. The corresponding  $V_{oc}$  is reported in Figure 4h. After 2000 working cycles in 1522 s, the output voltage of the AS-TENG remains stable with regard to

the initial state ( $V_{oc} = 110$  V), which indicates the AS-TENG has good durability and airtightness.

Based on the flexibility and waterproof properties of the AS-TENG, it can be applied to harvest mechanical energy from the motion of the fishtail. Since the main power of fish swimming is the force produced by the fishtail,<sup>[46]</sup> a bionic model has been designed to simulate the movement of the tail of a grass carp (*Ctenopharyngodon idellus*) (Figure S7, Supporting Information). Particularly, the design of multi-joints is the key for the model tail to have the ability to swing flexibly and simulate various movements of fish. The wearable AS-TENG with encapsulated LEDs has been placed on the fishtail model, and the system has been tested both in the air and underwater, respectively. The output performance of AS-TENG during the banding motion of the fishtail model has been studied both in the air (Figure 5a; Movie S2, Supporting Information) and underwater (Figure 5b; Movie S1, Supporting Information). The results show that the AS-TENG can convert the motion energy of the tail into electricity to light the LEDs. The contact and separation process of the AS-TENG can be clearly distinguished by the brightness of the LEDs in every oscillation, which obviously demonstrates the great flexibility and the mechanical responsiveness of the AS-TENG underwater. In addition, the output performance of the AS-TENG both in the air and underwater has been measured respectively, the output comparison results are shown in Figure 5c–e and Figure S8a–c (Supporting Information). Fatigue tests have been conducted on the

AS-TENGs after being manufactured for 7 months, while the AS-TENGs still show good mechanical sensitivity for energy harvesting and mechanical sensing. Attributed to the presence of the gaseous environment in the air sac, the AS-TENG exhibits stable output performance underwater.

Owing to its great mechanical responsiveness underwater, the AS-TENG is suitable for underwater fish behaviors monitoring. Instead of being attached to a fish body through surgical implantation, the flexible and skin-friendly FDSP is fixed on a fish by using a belt, which is inspired by the similar method of fixing a camera on a fish with the belt during underwater photography. Typical swimming gestures can be divided into two types: C-start and S-start, which are distinguished by the shape of the axis of the body during the initial locomotion.<sup>[47]</sup> In C-start, a large turning angle can be observed that makes the fish body curve into a C shape (Figure 6a), while the fish body curves into an S shape in S-start (Figure 6b).<sup>[48]</sup> To date, it is commonly believed that the C-start is mainly used in escape behavior and the S-start is adopted for prey capture.<sup>[49]</sup> However, as reported by Cheng et al., the behavior and performance of fish swimming may also show certain regularity

when they were exposed to polluted water.<sup>[50]</sup> Hence, it would be interesting to investigate fish swimming kinematics and the impact of environmental conditions through real-time monitoring signals. Since the maximum bending angle of the fishtail can reach 180°,<sup>[51]</sup> we have chosen 30°, 60°, 90°, and 120° as the basic angles for the test. In particular, a bend of 90° toward the opposite side in the C-start is also tested (Figure 6c, Figure Sa-b Supporting Information). Experimental results indicate that there is a relationship between the output performance of FDSP and the swing angle of the fishtail model, which is related to the difference of the gas flow inside the airbag that is affected by the oscillation angle. In addition, differences have also been found in output amplitudes and signal waveforms between C-start (Figure 6c; Figures S9a,b and S10a–c, Supporting Information) and S-start (Figure 6d, Figures S9c,d and S10d,e, Supporting Information), where the former displays an arch shape and the latter shows an S shape fluctuation. Besides, when turning angle is fixed at 90°, the output of FDSP at different frequencies for C-start and S-start motions of the fishtail is shown in Figure 6e,f, respectively.

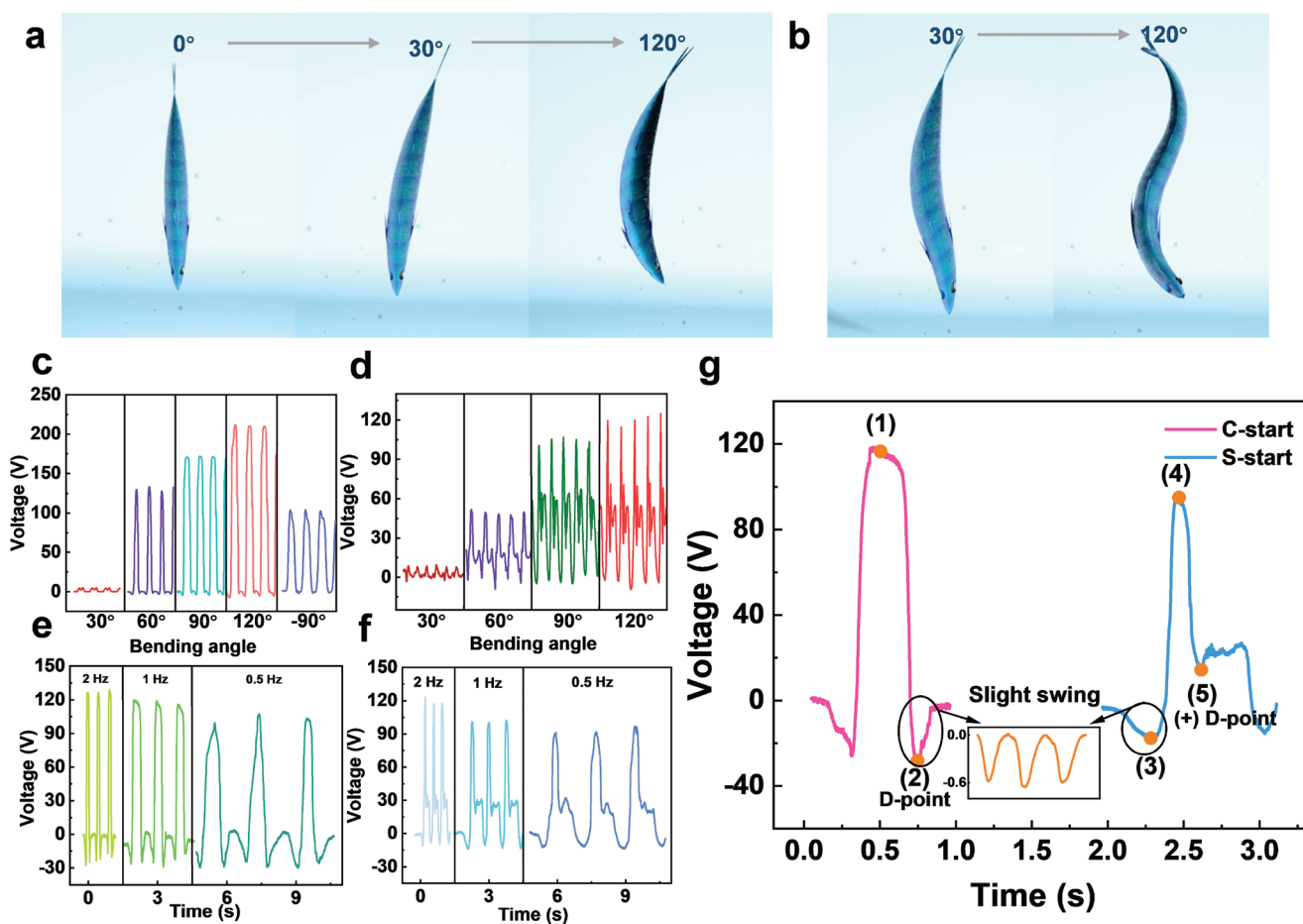


**Figure 6.** Working principle and electrical characteristics of the FDSP being used to measure the Fast-start behavior signals of fish. a) Schematic diagram of the different turning angles of fish during C-start motion. b) Schematic diagram of the different turning angles of fish during S-start. c)  $V_{oc}$  of FDSP when working at different bending angles ( $-90^\circ$ ,  $30^\circ$ ,  $60^\circ$ ,  $90^\circ$ ,  $120^\circ$ ) under C-start. d)  $V_{oc}$  of FDSP when working at different bending angles ( $30^\circ$ ,  $60^\circ$ ,  $90^\circ$ ,  $120^\circ$ ) under S-start.  $V_{oc}$  of FDSP at different working frequencies (2, 1, 0.5 Hz) during e) C-start and f) S-start. g) Comparison image of C-start and S-start signals in one cycle, the inset is the signal under slight swings (bending angle is  $0.5^\circ$ ).

The relationship between signal waveforms and Fast-start swimming (C-start and S-start motions) has been thoroughly investigated and the comparison graph of which within one cycle in the liquid environment is shown in Figure 6g. The signal from the C-start is a single peak, while the waveform in the S-start exhibits multiple peaks. To clearly distinguish the S-start from multiple continuous C-starts, the Diving-point (5) (D-point) is set as the key point of the S-start, which is defined as the lower point between two adjacent peaks in the signal diagram. The (+) D-point exists only in S-start and the value is positive, so it is easy to identify the moving gesture of fish by observing the presence or absence of the D-point in the signal waveform. On other hand, when fish make several isotropic or anisotropic C-start movements, the D-point is always a negative value, which can help to distinguish multiple C-start movements from S-start motion. The differences in signal waveforms between C-start and S-start are summarized

in Table S2 (Supporting Information). In addition, the FDSP has a high resolution for resolving the tiny angles of fishtailing. To reduce the obstruction of fish movement produced by FDSP, about 1 cm release at the caudal end of the sheath is reserved, which leads to the appearance of negative voltage at the onset of fish movement. As can be seen in the inset of Figure 6g, when the fishtail swings periodically with an oscillation amplitude of  $0.5^\circ$ , the output voltage of FDSP is 0.6 V.

With the help of a signal transmission module, a wireless monitoring system has been achieved as shown in Figure 7a. Here, we constructed the wireless transmission module with an electrometer data acquisition region (collect and process the signals from AS-TENG in real time) and a Bluetooth region (transfer signals to the receiver program), which is driven by a 5 V power supply module (Figure S11a, Supporting Information). The wireless transmission module is encapsulated in a small package made of silicone rubber to realize the water-proof

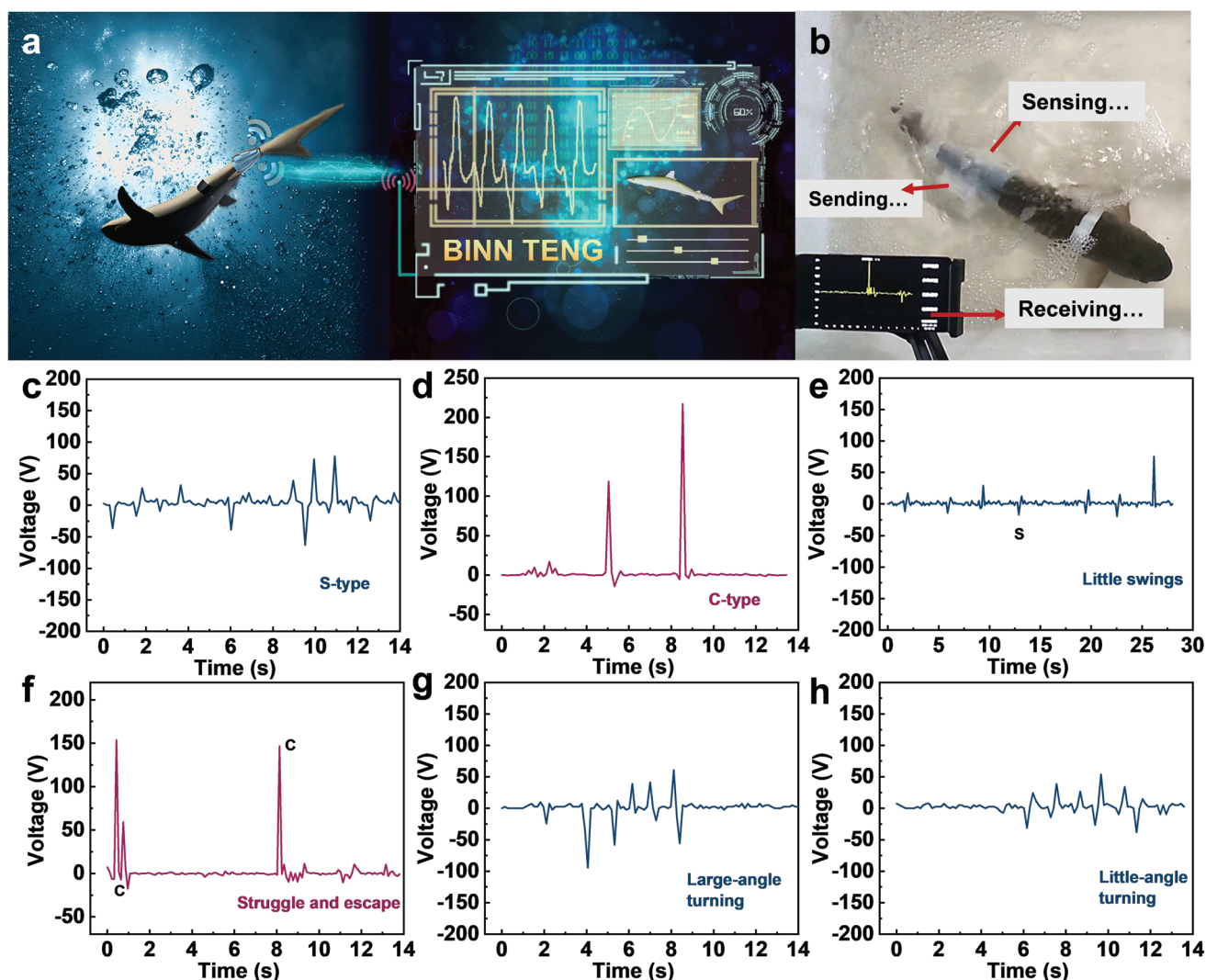


**Figure 7.** Underwater wireless fish-motion monitoring system based on FDSP. a) Schematic illustration of underwater wireless fish behavior monitoring system. b) Working schematic of the underwater wireless fish-motion monitoring system. Signal diagrams when fish moving in c) S-start and d) C-start. Signal diagrams of fish when it is under different moving states: e) little swings; f) struggle and escape; g) large-angle turning; and h) little-angle turning).

ability. The receiver program obtains post-processing functions such as fitting the signal (compensating for insufficient sampling rate), and finally displays the processed signal in real time. In this wireless FDSP, the data transmission module is powered by a battery, while the sensory module (AS-TENG) is fully self-powered, indicating an active sensory system with low energy consumption. With assistance from this wireless transmission module, FDSP can be integrated on the real fish (grass carp) in the water, completing its function as an underwater wireless motion sensor, the wireless transmission distance can reach about 1.2 m. The optical image of the FDSP system on a grass carp is shown in Figure 7b, where the FDSP is designed to be symmetrical on both sides to maintain the balance of the fish body. As can be seen in Figure 7c,d, the fish has a higher peak signal during C-start oscillation than that with S-start at the same motion angle, and the signal tends to increase as the turning angle increases, which is due to the less resistance to the airbag when the fishtail is under C-start movement. The signals of fish in some representative moving states, including Little swings, escaping state, and turnings, are also recorded by this wireless FDSP system, as shown in Figure 7e–h and Movie S4, Supporting Information). The detailed parameters of the obtained signals related to these moving states are summarized in Table S3 (Supporting Information). When the fish is in little swings, it mainly uses S-start oscillation and shows low frequency. Meanwhile, it takes high-frequency rapid C-start swings to escape from danger when the fish is stimulated to struggle or escape. A series of typical wireless signals from real fish with the swing gesture of C-start and S-start are selected and fitted via the interpolation method,<sup>[52]</sup> which can be seen in Figure S12a (Supporting Information) with good continuity. Based on the proposed analyzing method proposed in Figure 6g, the typical motion gesture of a real fish can also be distinguished from the output signal of FDSP. Figure S12b (Supporting Information) is a selected section of the signal generated from the free motion of fish in the water. It can be seen that the fish is in a fast continuous S-start oscillation at first and then, turns into a short C-start oscillation. After a resting state without oscillation, the fish finally performs slow S-start and C-start oscillations, which is consistent with the visual inspection. Here, the signal frequency corresponds to the pace of the fish swings, while the magnitude of the signal amplitude corresponds to the swing angle. By analyzing the various information obtained from FDSP, such as the signal waveform, the output amplitude and swing frequency, various behavioral rhythms, and physiological state of fish can be recorded.

### 3. Conclusions

In this work, an intelligent FDSP based on AS-TENG for remotely monitoring the swing motion of a fishtail has been proposed for the first time. The device has been integrated with multiple functions of disinfection, mechanical energy harvesting, real-time monitoring, and wireless data transmission, focusing on underwater cases. Different from human-wearable TENG, the interference from the external environment can be effectively reduced by the full-encapsulated strategy, greatly

improving the durability and stability. The flexible air sac structure also provides a proper buoyancy to reduce the obstruction to the movement of fish. By applying mechanical stress to the airbag, the airflow can circulate in the AS-TENG and induce contact-separation motion of TENG to produce output signals. With each swing of the fishtail, the AS-TENG can provide a peak output voltage of 150 V and a peak output power of 0.74 mW, which is possible to power up some tiny electronic devices. When integrated into the fish, the output voltage from AS-TENG can also be used to precisely detect the swinging and turning motion of the fishtail, where the highest resolution of the detected turning angle can reach 0.5°. The wireless communication system is designed to transmit the sensory data to a cell phone and the remote monitoring of fish motion can be achieved. Here, the data transmission module is powered by a battery, while the sensory module (AS-TENG) is fully self-powered, indicating an active sensory system with low energy consumption. By analyzing key parameters of the output voltage such as  $V_{(1)}$ ,  $V_{(4)}$ , and the D-point between two voltage peaks, the detailed information about the fish swimming, such as the swing frequency, swing angle, and even the gesture of the fishtail, can be accurately distinguished. The antimicrobial coating on the rubber sleeve has the advantages of low cost, effective sterilization, and little pollution to the environment, which can improve the biocompatibility of FDSP. Different from the traditional methods using images or acoustic waves to study fish kinematics, this FDSP can achieve a real-time and wireless monitoring of fish behaviors in a blind view. Hence, this FDSP may greatly facilitate the study of fish behavior and its neural basis in different species, while the similar design concept can also inspire a series of potential applications in undersea robotics, wearable tracking devices, and eco-friendly sensors.

### 4. Experimental Section

**Materials:** The silicone (Ecoflex™ 00 30) was produced by Smooth-On. The PDMS was made by Dow Corning. The 42% Sodium Silicate was from Atech Chemical Co. 80% DDAC was from Aladdin Reagent. A 3D printer (Raize 3D) and polylactic acid (PLA) printing supplies were used to design and print the fishtail model (30 cm in length), which were designed equivalent to a real grass carp (about 70 cm in length). Custom-sized acrylic molds were used as containers for curing the components of FDSP. Green commercial LEDs were used as underwater appliances to verify the energy conversion of the FDSP.

**Preparation of Antibacterial Coating:** First, the Fixed-Quat coating agent was prepared. Sodium silicate (42%, 53 ml) combined with DI water (910 ml) were mixed thoroughly and stirred at 150 rpm for 6 h at room temperature using a magnetic stirrer until fully dissolved. Then, DDAC solution (80%, 18.75 ml) was added dropwise and stirred for 24 h until well mixed. The final concentration of the Fixed-Quat agent was 13500 (w/v). Second, clean silicone rubbers were immersed into the Fixed-Quat solution on a platform shaker and mixed at 150 rpm for 20 h. Finally, the samples were carefully taken out, gently rinsed with DI water, followed by oven-drying at 50 °C for 20 h.

**Structure Design and Fabrication of AS-TENG:** The AS-TENG was prepared by the split method. First, after precise calculation of the size, acrylic sheets were used to prepare the various molds required in the experiment. Then, the silicone was prepared by mixing the required quantities of A component and B component of Ecoflex™ 0030 in a container (1A:1B by volume or weight), stirring until well mixed. The mixture was placed in a vacuum oven for vacuum degassing until the mixture was free of air bubbles. The vacuum-degassed mixture

was poured into the upper and lower component molds and cured at 60 °C for 1 h. The cured silicone components were removed from the molds. The wires and aluminum foil electrodes were attached to the air chambers on both sides of the upper silicone component, and the opposite wires and aluminum foil electrodes covered with PTFE film were attached to the air chambers on both sides of the lower silicone component correspondingly. The upper and lower silicone components with the electrodes and the friction layer adhered were aligned face to face in the designed mold, and a thin layer of unformed silicone was applied on the contact surface and outside of the components. After curing at 60 °C for 1 h, a complete airbag was formed by the combination of the two components. Finally, magnet sheets were attached to the corresponding sides of the electrodes and were encapsulated with silicone again.

**Fabrication of Mechanical Energy Harvesting System Based on the AS-TENG:** Flexible silicone sleeves that can carry AS-TENG and electrical appliances were manufactured first. The unformed silicone gel was poured into a customized mold of fishtail size and cured at 60 °C for 1 h. The cured silicone sleeve was removed and dropped in a Fixed-Quat coating agent to stirring for 24 h. Afterward, ten LEDs in series were connected to the outputs of the AS-TENG, both the LEDs and exposed wires were encapsulated with PDMS. Finally, the encapsulated LEDs and AS-TENG were fixed on the silicone sleeve by applying the unformed silicone gel and cured in an oven at 60 °C for 1 h.

**Fabrication of the Wireless FDSP:** The FDSP was constructed by the combination of an antimicrobial rubber sleeve, an AS-TENG, a power supply, and a wireless signal transmission module. The power supply and the wireless transmission module were encapsulated together in a sealed box made of silicone. The AS-TENG and the wireless transmission module were directly connected by varnished wires and the exposed wires and the gap between the silicone box is sealed with silicone gel. The AS-TENG and silicone box were fixed to the rubber sleeve with silicone gel and placed in an oven at 60 °C for 1 h. The information collected by the real-time fish behavior monitoring system would be transmitted to a mobile phone or computer through a wireless receiver, and the received real-time signal can be displayed through an open-source software.

**Characterization and Measurement:** All the experiments related to bacteria were performed in the biosafety cabinet. The open-circuit voltage, short-circuit current, and short-circuit charge of the AS-TENG were measured with a Keithley 6514 electrometer. Mechanical stretching and frequency tests of the AS-TENG were performed by a linear motor (LinMot E1100) for periodic and continuous mechanical traction of AS-TENG. The output performance of AS-TENG at different frequencies and different stretching rates was measured by setting different speeds and distances of the linear motor. A mechanical angle controller was used to measure the output performance of the AS-TENG at different angles. The underwater output of the AS-TENG was measured by connecting the Keithley 6514 electrometer to the AS-TENG with a waterproof wire. In addition, a wireless signal transceiver module was used to record the underwater signals from the FDSP. Scanning electron microscopy imaging was performed by a Hitachi emission scanning electron microscope (SU 8020) equipped with an EDS probe.

**Experiments with Animal Subjects:** The motion behavior of grass carp was studied by using this FDSP. The experiments with these animal subjects had been performed in compliance with all the ethical regulations under a protocol that was approved by the Institutional Review Board at Beijing Institute of Nanoenergy and Nanosystems, Chinese Academy of Sciences.

## Supporting Information

Supporting Information is available from the Wiley Online Library or from the author.

## Acknowledgements

This work was supported by the National Natural Science Foundation of China (Grant No. 62174014), Beijing Natural Science Foundation (4192069), the Beijing Municipal Science & Technology Commission (Z171100000317001), Young Top-Notch Talents Program of Beijing Excellent Talents Funding (2017000021223ZK03), Beijing Nova Program (Z201100006820063), and Youth Innovation Promotion Association CAS (2021165).

## Conflict of Interest

The authors declare no conflict of interest.

## Data Availability Statement

The data that support the findings of this study are available from the corresponding author upon reasonable request.

## Keywords

antibacterial coating, blue energy, fish kinematics, self-powered sensors, triboelectric nanogenerators

Received: November 22, 2021

Revised: December 30, 2021

Published online:

- [1] L. C. Rome, D. Swank, D. Corda, *Science* **1993**, 261, 340.
- [2] T. M. Schaerf, P. W. Dillingham, A. Ward, *Sci. Adv.* **2017**, 3, e1603201.
- [3] P. Domenici, M. E. Hale, *J. Exp. Biol.* **2019**, 222, jeb166009.
- [4] B. N. Nowroozi, E. L. Brainerd, *Zoology (Jena)* **2014**, 117, 28.
- [5] J. C. Liao, O. Akanyeti, *Mar. Technol. Soc. J.* **2017**, 51, 48.
- [6] J. Zhu, C. White, D. K. Wainwright, V. Di Santo, G. V. Lauder, A. H. Bart-Smith, *Sci. Robot.* **2019**, 4, 4615.
- [7] S. B. Yang, Q. Jing, X. Y. Han, *J. Bionic Eng.* **2009**, 6, 174.
- [8] L. Li, M. Nagy, J. M. Graving, J. Bak-Coleman, I. D. Couzin, *Nat. Commun.* **2020**, 11, 1.
- [9] U. Müller, J. Leeuwen, *Fish Fish (Oxf)* **2010**, 7, 84.
- [10] F. Berlinger, M. Gauci, R. Nagpal, *Sci. Robot.* **2021**, 6, eabd8668.
- [11] W. Liu, N. Li, J. Zhao, Y. Su, *Saudi J. Biol. Sci.* **2016**, 24, 1344.
- [12] M. I. McCormick, E. P. Fakan, S. L. Nedelec, B. J. M. Allan, *Sci. Rep.* **2019**, 9, 6554.
- [13] D. J. Coughlin, *J. Exp. Biol.* **2000**, 203, 617.
- [14] S. Cheng, K. Zhao, D. Zhang, *Symmetry* **2019**, 11, 1179.
- [15] I. Masmijta, J. Navarro, G. A. K. O'Reilly, K. Katija, J. B. Fannjiang, *Sci. Robot.* **2020**, 5, 3701.
- [16] Z. L. Wang, J. Song, *Science* **2006**, 312, 242.
- [17] Z. L. Wang, *Adv. Energy Mater.* **2020**, 10, 2000137.
- [18] F. Wang, J. Tian, Y. Ding, Y. Shi, X. Tao, X. Wang, Y. Yang, X. Chen, Z. L. Wang, *iScience* **2021**, 24, 102502.
- [19] J. Nie, X. Chen, L. W. Zhong, *Adv. Funct. Mater.* **2019**, 29, 1806351.
- [20] F. Wang, Z. Ren, J. Nie, J. Tian, Y. Ding, X. Chen, *Adv. Mater. Technol.* **2020**, 5, 1900789.
- [21] L. Jin, W. Deng, Y. Su, Z. Xu, H. Meng, B. Wang, H. Zhang, B. Zhang, L. Zhang, X. Xiao, M. Zhu, W. Yang, *Nano Energy* **2017**, 38, 185.
- [22] Q. Gao, T. Cheng, Z. L. Wang, *Extreme Mech. Lett.* **2021**, 42, 101100.

- [23] R. Lei, Y. Shi, Y. Ding, J. Nie, S. Li, F. Wang, H. Zhai, X. Chen, Z. L. Wang, *Energy Environ. Sci.* **2020**, *13*, 2178.
- [24] H. L. Cheng, L.-F. Zhao, J. Xiao, P. Gao, P. Wen, W.-C. Zhou, H.-L. Du, *Rare Met.* **2019**, *38*, 1193.
- [25] X. L. Fan, Y. F. Huo, C. Y. Li, M. B. Kannan, X. B. Chen, S. K. Guan, R. C. Zeng, M. Q. L., *Rare Met.* **2019**, *38*, 520.
- [26] C. Dong, M. Li, T. Yang, L. Feng, Y.-W. Ai, Z.-L. Ning, M.-J. Liu, X. Lai, D.-J. Gao, *Rare Met.* **2021**, *40*, 505.
- [27] X. Tao, S. Li, Y. Shi, X. Wang, J. Tian, Z. Liu, P. Yang, X. Chen, Z. L. Wang, *Adv. Funct. Mater.* **2021**, *31*, 2106082.
- [28] F. R. Fan, Z. Q. Tian, Z. L. Wang, *Nano Energy* **2012**, *1*, 328.
- [29] Y. Zou, P. Tan, B. Shi, H. Ouyang, Z. Li, *Nat. Commun.* **2019**, *10*, 2695.
- [30] Y. Su, C. Chen, H. Pan, Y. Yang, G. Chen, X. Zhao, W. Li, Q. Gong, G. Xie, Y. Zhou, S. Zhang, H. Tai, Y. Jiang, J. Chen, *Adv. Funct. Mater.* **2021**, *31*, 2010962.
- [31] Y. Su, G. Chen, C. Chen, Q. Gong, G. Xie, M. Yao, H. Tai, Y. Jiang, J. Chen, *Adv. Mater.* **2021**, *33*, 2101262.
- [32] Y. Su, W. Li, L. Yuan, C. Chen, H. Pan, G. Xie, G. Conta, S. Ferrier, X. Zhao, G. Chen, H. Tai, Y. Jiang, J. Chen, *Nano Energy* **2021**, *89*, 106321.
- [33] Z. Wang, J. An, J. Nie, J. Luo, J. Shao, T. Jiang, B. Chen, W. Tang, Z. L. Wang, *Adv. Mater.* **2020**, *32*, 2001466.
- [34] J. A. Rogers, T. Someya, Y. Huang, *Science* **2010**, *327*, 1603.
- [35] L. Jin, X. Xiao, W. Deng, A. Nashalian, J. Chen, *Nano Lett.* **2020**, *20*, 6404.
- [36] M. Macias, I. F. Souza, A. Junior, T. F. Oliveira, *Mech. Res. Commun.* **2020**, *107*, 103547.
- [37] E. Vinepinsky, L. Cohen, S. Perchik, O. Ben-Shahar, R. Segev, *Sci. Rep.* **2020**, *10*, 14762.
- [38] L. E. N. Adler, M. I. McCormick, J. L. Johansen, P. Domenici, *Commun. Biol.* **2021**, *4*, 1.
- [39] Y. C. Liu, M. E. Hale, *Curr. Biol.* **2017**, *27*, 697.
- [40] Y. Zhu, F.-B. Tian, J. Young, J. C. Liao, J. C. S. Lai, *Sci. Rep.* **2021**, *11*, 1691.
- [41] K. Hegstad, S. Langsrud, B. T. Lunestad, A. A. Scheie, M. Sunde, S. P. Yazdankhah, *Microb. Drug Resist.* **2010**, *16*, 91.
- [42] D. Diaz, J. Church, M. Young, K. T. Kim, J. Park, Y. B. Hwang, S. Santra, W. H. Lee, *J Environ Sci (China)* **2019**, *82*, 213.
- [43] J. M. Baik, J. P. Lee, *Sci. Technol. Adv. Mater.* **2019**, *20*, 927.
- [44] Y. Fan, S. Li, X. Tao, Y. Wang, Z. Liu, H. Chen, Z. Wu, J. Zhang, F. Ren, X. Chen, E. Fu, *Nano Energy* **2021**, *90*, 106574.
- [45] Z. L. Wang, *Mater. Today* **2017**, *20*, 74.
- [46] I. Borazjani, *Integr. Comp. Biol.* **2015**, *55*, 740.
- [47] O. Akanyeti, P. J. M. Thornycroft, G. V. Lauder, Y. R. Yanagitsuru, A. N. Peterson, J. C. Liao, *Nat. Commun.* **2016**, *7*, 11044.
- [48] P. Domenici, R. W. Blake, *J. Exp. Biol.* **1997**, *200*, 1165.
- [49] C. Lefrancois, M. Cannas, P. Morniere, P. Domenici, *Comp. Biochem. Physiol., Part A: Mol. Integr. Physiol.* **2007**, *146*, S125.
- [50] G. G. Sass, P. J. Motta, *Environ. Biol. Fishes* **2002**, *65*, 441.
- [51] W. C. Witt, L. Wen, G. V. Lauder, *Integr. Comp. Biol.* **2015**, *55*, 728.
- [52] S. Niu, Y. Liu, S. Wang, L. Lin, Y. S. Zhou, Y. Hu, Z. L. Wang, *Adv. Mater.* **2013**, *25*, 6184.